

# Overmoded GW-Class Surface-Wave Microwave Oscillator

Alexander N. Vlasov, *Member, IEEE*, Anatoly G. Shkvarunets, John C. Rodgers, Yuval Carmel, *Senior Member, IEEE*, Thomas M. Antonsen, Jr., *Member, IEEE*, Tamer M. Abuelfadl, *Student Member, IEEE*, Duan Lingze, Vladimir A. Cherepenin, *Member, IEEE*, Gregory S. Nusinovich, *Fellow, IEEE*, Moti Botton, and Victor L. Granatstein, *Fellow, IEEE*

**Abstract**—Results of theoretical and experimental studies of a GW-class, large diameter microwave oscillator are presented. The device consists of a large cross-section (overmoded), slow-wave structure with a unique profile of wall radius specifically designed to support surface waves and to provide a strong beam-wave coupling at moderate voltage (500 kV), an internal adjustable microwave reflector, a coaxial microwave extraction section, and a coaxial magnetically insulated field emission electron gun. In preliminary experiments carried out at 8.3 GHz, the power level exceeding 0.5 GW and efficiency of 15% have been measured calorimetrically.

**Index Terms**—High-power microwave (HPM), overmoded, surface-wave oscillator.

## I. INTRODUCTION

APPLICATIONS of high-power microwave (HPM) devices capable of generating gigawatt (GW) levels of output power at centimeter wavelengths include directed-energy warfare, laboratory sources for the vulnerability, and susceptibility testing of electronic systems. However, the maximum peak-power handling capability of HPM sources is severely limited by internal microwave breakdown [1].

One method of increasing the power-handling capabilities of HPM devices is to increase their transverse diameter  $D$  to several times free-space wavelength  $\lambda$  thereby reducing the internal field stress for the same power flow. For a  $TM_{m,p}$  mode propagating in a smooth-wall cylindrical waveguide the relation between the maximum power  $P_{\max}$  and maximum strength of the

electric field allowable at the wall,  $E_{\max,w}$ , can be given by

$$P_{\max}[\text{GW}] = 8.707(1 + \delta_{0,m}) \left( \frac{E_{\max,w} \left[ \frac{\text{kV}}{\text{cm}} \right] \lambda[\text{cm}]}{511} \right)^2 \times \frac{\pi^2}{4} D'^4 \sqrt{1 - \left( \frac{\nu_{m,n}}{2\pi D'} \right)^2} \frac{1}{\nu_{m,n}^2} \quad (1)$$

where  $D' = \pi D/\lambda$ ,  $\lambda$  is the free-space wavelength,  $\nu_{m,p}$  are roots of equation:  $J_m(x) = 0$ ,  $J_m(x)$  is Bessel function of order  $m$ ,  $\delta_{0,m}$  is equal to 1 if  $m = 0$  and equal to 0 in other cases. This oversized approach has been successfully used to increase the power handling capabilities of slow-wave HPM sources [2]–[4]. By using this method, microwave-generating structures can be designed with internal microwave electric fields below the breakdown levels. Consider, for example, the maximum propagating power that can be supported by a smooth-wall circular waveguide operating at the transverse magnetic  $TM_{01}$  mode at 8.2 GHz assuming that the maximum allowable electric field at the wall is  $E_{\max,w} = 100$  kV/cm. Under these conditions, as follows from (1), the waveguide can support a maximum propagating power of 1 GW when  $D/\lambda \approx 1.7$ . Note that the power handling capability of lowest symmetrical mode  $TM_{01}$  is maximal among the TM modes.

Oversized slow-wave generators have produced record levels of multi-GW microwave radiation. The relativistic diffraction generator [5] demonstrated a peak output power of 4.5 GW in the 9–11.3 mm wavelength range and the multiwave Cerenkov generator [6] has produced 15 GW at a wavelength of 3 cm. These results were achieved by using a high-voltage electron beam (in the range of 1.5–2 MV). For practical devices, operation at reduced voltages, possibly no more than 500 kV, is preferable. So far, the maximum power achieved in slightly oversized backward wave oscillator (BWO) with  $D/\lambda \approx 1.8$  operating at 550 kV is about 0.8 GW at 10-GHz frequency [7].

In this work, we present an investigation of an HPM device with an overmoded slow-wave structure. We designed and experimentally tested a large diameter ( $D/\lambda \cong 3$ ), high-power, high-efficiency, microwave source operating at 8.3 GHz. The unique features of this generator are 1) a slow-wave structure (SWS) with a complex profile specifically designed to support surface waves and to provide strong beam-wave coupling at 500 kV, 2) an adjustable internal reflector for power, efficiency and frequency tunability, 3) a coaxial output coupler for efficient axial energy extraction, and 4) a coaxial magnetically insulated

Manuscript received October 19, 1999; revised February 1, 2000. This work was supported by the Air Force Office of Scientific Research, MURI Research on "Compact, High-Energy, Microwave Sources," and by the Office of Naval Research.

A. N. Vlasov is with the Science Applications International Corporation, McLean, VA 22102 USA, on leave from Moscow State University, Moscow, Russia.

A. G. Shkvarunets, J. C. Rodgers, Y. Carmel, T. M. Antonsen, Jr., T. M. Abuelfadl, D. Lingze, G. S. Nusinovich, and V. L. Granatstein are with the Institute for Plasma Research, University of Maryland, College Park, MD 20742 USA.

V. A. Cherepenin is with the Institute of Radio Engineering and Electronics, Russian Academy of Sciences, Moscow 103907, Russia.

M. Botton is with Rafael, P.O. Box 2250, Haifa, Israel.

Publisher Item Identifier S 0093-3813(00)05377-7.

field emission electron gun with a variable anode–cathode gap. Section II describes the basic concept of a large diameter surface wave generator, as well as the actual design. The experimental results are presented in Section III. A summary of the results and conclusions are given in Section IV.

## II. BASIC CONCEPT OF A LARGE DIAMETER SURFACE-WAVE GENERATOR

### A. General Considerations

The goal of current research was to design and test a GW-class device operating at a relatively low voltage of about 500 kV. The operating voltage also determines a maximum beam current, which can be transmitted through a cylindrical waveguide [8]. The maximum beam power of a thin annular electron beam of radius  $r_b$  propagating in a waveguide of a radius  $r_{aw}$  can be given by

$$P_{b, \text{Lim}}[\text{GW}] = \frac{8.707}{2 \ln(r_w/r_b)} W(\gamma_a) \gamma_a^2 \quad (2)$$

where  $\gamma_a = 1 + eV_{ac}/mc^2$  corresponds to the anode-cathode voltage  $V_{ac}$ , the function  $W(\gamma_a)$  describes the voltage depression effect discussed elsewhere [8]. A short derivation of expression (2) and a graph of  $W(\gamma_c)$  are presented in Appendix A. The maximum beam power increases when the beam is streaming close to the wall ( $r_b \cong r_{aw}$ ). To avoid beam interception a practical requirement is  $(r_w - r_b) \approx 0.5$  cm. So, to substantially increase the beam power, both beam and wall radii should be increased simultaneously. In order to generate output power of about 1 GW, assuming a beam-microwave conversion efficiency of  $\eta = 20\%$ , the required beam power is 5 GW. At 500 kV and for  $(r_w - r_b) = 0.5$  cm, the wall radius is  $r_{aw} \approx 3.5$  cm, and  $W = 0.047$ . This corresponds to  $D/\lambda \sim 2$  for 8.3 GHz operation. These considerations provided initial motivation for our choice of the operating parameters.

Linear beam relativistic microwave devices are based on the interaction between an electron beam and an electromagnetic field containing slow-wave components. Such a field can be realized in spatially periodic structures. The eigenmodes of an infinite periodic structure can be used as first approximation to describe the electromagnetic field of a finite length slow-wave structure. The electromagnetic field components of an eigenmode at frequency  $\omega$  can be expressed as an infinite sum over spatial harmonics

$$E_z = \sum_{n=-\infty}^{\infty} a_n G_m(k_{\perp, n} r) e^{im\theta} e^{ik_{z, n} z} e^{-i\omega t} + \text{c.c.} \quad (3)$$

where

$$k_{z, n} = k_{z, 0} + \frac{2\pi}{d} n, \quad n = 0, \pm 1, \pm 2, \dots$$

$d$  is period of the structure,  $m$  is the azimuthal index of eigenmode,  $n$  is the spatial harmonic number, and  $\theta$  is azimuthal coordinate. The transverse and longitudinal wave numbers satisfy the equation (for each  $m$ )

$$k_{z, n}^2 + k_{\perp, n}^2 = \left(\frac{\omega}{c}\right)^2. \quad (4)$$

The transverse distribution of electromagnetic field depends on the relationship between  $\omega/c$  and longitudinal wavenumber. If  $|k_{z, n}^{(m, p)}| < \omega/c$ , the spatial harmonic is fast and volumetric since its field profile is described by the ordinary Bessel function of order  $m$ ,  $G_m = J_m$ . However, when  $|k_{z, n}^{(m, i)}| > \omega/c$ , the harmonic is slow, and the field profile is described by the modified Bessel function of order  $m$ , namely  $G_m = I_m$ . The field of this harmonic is localized near the surface of SWS. In the general case, an eigenmode of a periodic waveguide consists of both fast and slow spatial harmonics. However, it is possible to design a periodic structure for which the selected eigenmode in a certain frequency range consists of only slow spatial harmonics. In this case, the eigenmode is a surface wave, as discussed elsewhere [9], and it plays an important role in the realization of large diameter microwave sources.

### B. Mode Selection in Oversized Surface-Wave Generators

The interaction region of relativistic microwave generators is often composed of a spatially periodic SWS connected to a smooth waveguide. Mode selection is usually not an issue in devices having relatively small transverse cross-section,  $r_w < 0.5\lambda$ , since these devices operate in low-order modes. However, this issue becomes increasingly complicated when the transverse size of structure becomes larger, e.g., several times the operating wavelengths,  $r_w \sim (2 \div 3)\lambda$ . In infinitely long nonovermoded systems the dispersion curves for different transverse modes are well separated in frequency (passbands are separated by stop bands). In finite-length, nonovermoded structures with large end reflections, the  $Q$ -factors of eigenmodes are high, so that the axial modes are also well separated in frequency.

When overmoded structures are considered, the situation is quite different. The dispersion curves for different transverse modes may overlap in frequency (they are not separated by stop bands). Furthermore, overmoded structures are often characterized by small end reflections of eigenmodes located far from passband edges (low  $Q$ -modes), and therefore neighboring longitudinal modes can also overlap in frequency. Thus, to design an oversized BWO, a very complicated problem should be solved, namely, to provide some form of mode selection. Some successful designs based on using a selective Bragg reflector for the desired mode were described in [10] and [11].

Another approach was suggested in [12]. This method achieves mode selection in oversized structures by shifting the operating point close to upper edge of the passband. In this region, the  $Q$ -factor is relatively large due to both large the reflection and small group velocity, as can be seen from the equation for the diffraction quality factor,  $Q_{\text{diff}}$

$$Q_{\text{diff}} = \frac{\omega L}{v_{gr}(1 - |R|)} \quad (5)$$

where  $\omega$ ,  $v_{gr}$ ,  $R$ , and  $L$  are the angular frequency, group velocity, reflection coefficient, and total length of the structure, respectively. In accordance with this idea, we choose an operating point close to the upper edge of the band to provide mode selection. Since the desired operating voltage is relatively low (500 kV), the corresponding phase velocity for the synchronous spatial harmonic should be close to, but below, the

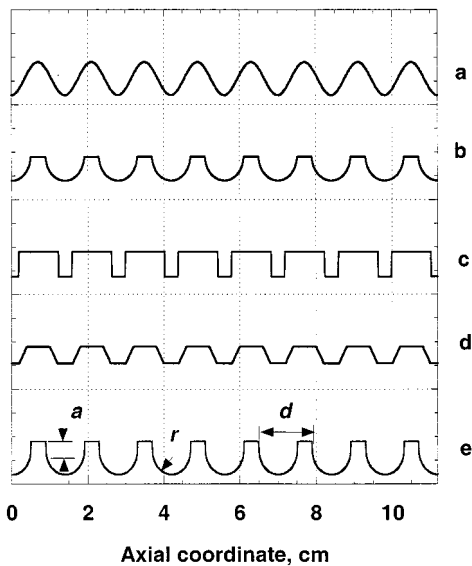


Fig. 1. The examples of wall radius profiles as functions of axial coordinate.

beam velocity. These two requirements (operating near  $\pi$  point and phase velocity below  $0.85c$  when  $\gamma < 2$ ) lead us to the surface-wave approach.

### C. Choosing a Profile for the Slow Wave Structure

The main goal is to find a SWS profile capable of 1) supporting slow waves with phase velocity below that of a 500-kV electron beam, and 2) ensuring strong enough coupling impedance over the frequency range of interest (8.5 GHz) for a beam located relatively far from the structure's surface. In order to meet these requirements, various axial profiles of wall radius for the periodic structure were analyzed, namely, sinusoidal, rectangular, trapezoidal, semicircular, and a combination of rectangles and semicircles. Examples of these are illustrated in Fig. 1.

In this study, performed numerically using the WAVESIM computer code [13], the dispersion diagram for the lowest transverse mode of each periodic oversized structure was constructed using the technique described in [14]. The search was limited to relatively small amplitude of corrugations,  $h < \lambda/4$ , in order to provide good beam transport through the structure. Under these conditions, smooth profiles, such as sinusoidal and semicircle, examples in Fig. 1(a) and (b) were not found to provide enough slowing of the wave and adequate coupling impedance. Rectangular or trapezoidal profiles, examples in Fig. 1(c) and (d) are better, but are characterized by unacceptably strong electric fields near the sharp edges. A spatially periodic structure composed of semicircles on top of rectangles was found to simultaneously satisfy both requirements (slow wave and strong coupling). See this example in Fig. 1(e). The period  $d$ , the radius of semicircles  $r$ , and the depth of rectangular corrugations  $a$  were varied to find an optimal profile of periodic structure. The optimization included several steps. First, the structure period  $d$  was chosen to provide an interaction between the lowest mode and 500-kV electron beam in the frequency region from 8 to 9 GHz. Second, the radius of semicircles  $r$  was optimized to achieve the maximum value of coupling coefficient.

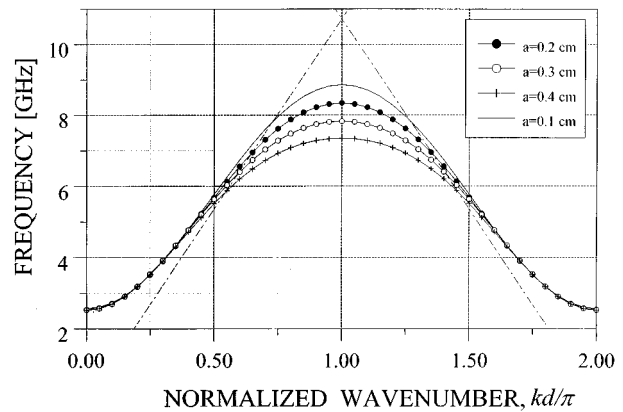


Fig. 2. Calculated dispersion diagram for  $TM_{0,1}$  mode in a periodic, oversized structure. Four curves correspond to different amplitude of rectangular grooves (in all cases, minimal radius is 4.2 cm; period is 1.4 cm; semicircle radius is 0.5 cm). The dotted line is the light line.

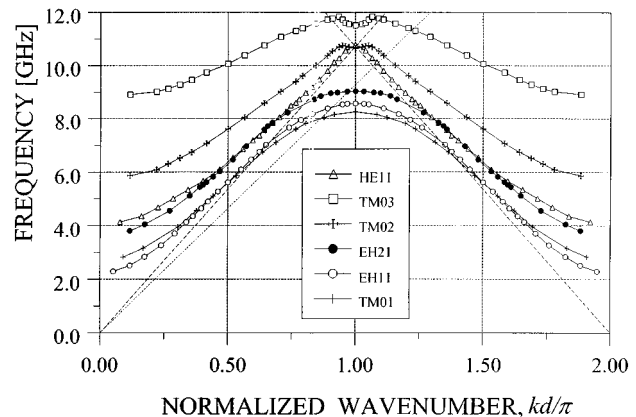


Fig. 3. Calculated dispersion diagrams for six lowest modes of periodic oversized structure with optimal profile (maximal radius 4.9 cm; period 1.4 cm; height of rectangles 0.2 cm; radius of semicircle 0.5 cm). Light line—dashed, 511 kV beam line—dotted.

The dispersion diagrams of the lowest symmetric mode for the optimal period,  $d = 1.4$  cm, and the optimal radius of semicircles,  $r = 0.5$  cm, are shown in Fig. 2. The different curves are correspondent to different values of rectangular groove depth. In this case, it is possible to independently control the boundaries of the passband. The profile amplitude determines the upper cutoff almost exclusively, while the lower cutoff is determined by the waveguide diameter.

The dispersion diagrams of the  $TM_{01}$ ,  $TM_{02}$ ,  $TM_{03}$ ,  $EH_{11}$ ,  $HE_{11}$ , and  $HE_{21}$  modes for the optimal structure are presented on Fig. 3, as calculated by using the SHOOTER code based on the method presented in [15]. The dashed line in Fig. 3 represents the beam Doppler line, and the operating point will be in the vicinity of  $k_z d \cong \pi$  and  $f \cong 8.2$  GHz. The Doppler line of 500-kV electron beam crosses the dispersion curves of the higher order symmetric modes ( $TM_{02}$ ,  $TM_{03}$ ) at frequencies about 10 GHz, which are significantly higher than the operating frequency for  $TM_{01}$  mode. Note that the dispersion curve of  $EH_{11}$  mode lies near the selected operating point of  $TM_{01}$  mode. We will discuss later the relationship between starting currents of  $EH_{11}$  and  $TM_{01}$  modes and show how the axially symmetric mode  $TM_{01}$  can be selected.

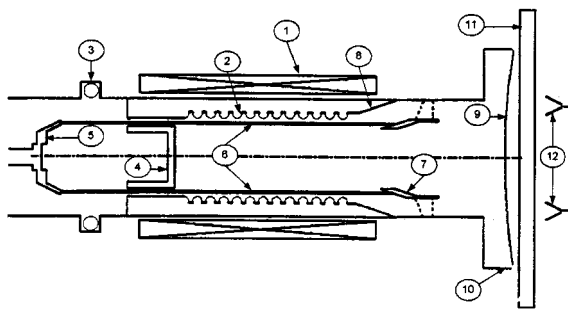


Fig. 4. A schematic diagram of the large diameter, surface-wave generator: 1—solenoid, 2—slow wave overmoded structure, 3—Rogowsky current monitor, 4—adjustable RF reflector, 5—explosive cathode, 6—electron beam, 7—coaxial collector, 8—output up-taper, 9—output window, 10—vacuum jacket, 11—wide-band calorimeter, 12—receiving horns, connected to hot carrier detectors.

#### D. Eigenmodes of an Oversized Open Resonator and the Influence of an Internal Reflector

The layout of the experimental device is shown in Fig. 4. The interaction circuits of 12.5 periods of the structure are analyzed in Fig. 3. The beam enters from the left and passes a moveable reflecting surface. On the right, the structure connects to a straight section of waveguide and then an up taper. The beam is collected on the coaxial graphite collector. An internal reflector separates the radio frequency (RF) interaction region from the electron gun. It serves both to reflect the microwave power and to control the longitudinal distribution of the field. The electron beam was injected through an array of 12 thin-wall, stainless steel tubes (0.9-cm diameter, 5-cm long) mounted in an annular slit in the reflector. This arrangement proved to be a transparent coaxial tunnel for beam injection, and a good microwave reflector for frequencies up to  $\sim 14$  GHz. The axial position of the reflector is continuously adjustable.

Studies of a small diameter backward wave oscillator using a cutoff reflector separated from the beginning of SWS by a smooth waveguide section was described in [16], and the BWO operation as well as a small diameter SWS properties near the  $\pi$  point were studied in [17]. It was found that moving the reflector could modify the performance of the device (namely, operating frequency and efficiency). In the present case, the situation will be somewhat different due to the fact that we are considering an overmoded structure. As a consequence, fields in the structure do not match directly those in the straight section, which are above cutoff. Consequently, varying the location of the shortening plate does not continuously vary the phase of the reflection coefficient of at the boundary of structure.

The properties of this structure were therefore studied numerically using, again, the code WAVESIM. In the simulations, the output taper was replaced by a straight section of waveguide that was terminated by a boundary on which the boundary condition enforced outgoing waves. Further, fields were excited in the structure by a current source (or antenna) whose frequency could be specified. Simulations for a range of frequencies and a range of locations of the reflector were performed. Fig. 5 shows plots of the magnitude of the azimuthal magnetic field,  $|H_\theta|$ , versus frequency for two different locations of the reflector ( $\Delta z = 0$  mm and  $\Delta z = 10$  mm). The plots indicate

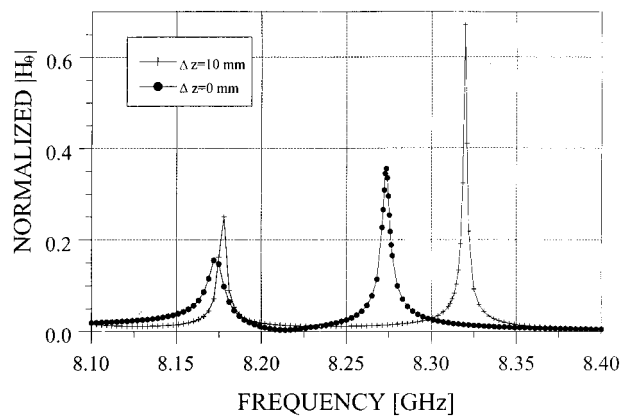
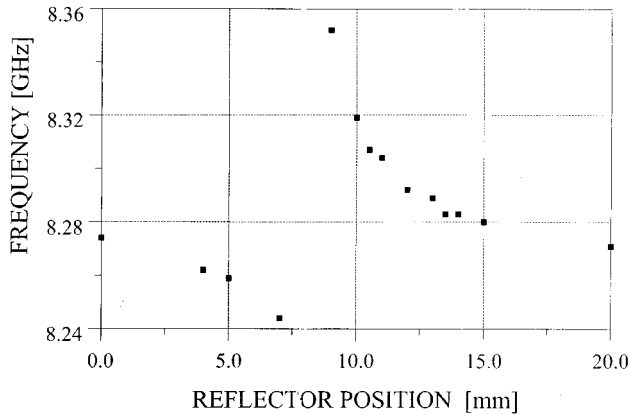


Fig. 5. Calculated dependence of electromagnetic field magnitude  $H_\theta$  on frequency for oversized open resonator with 12 periods with optimal profile (maximal radius 4.9 cm, period 1.4 cm, height of rectangles 0.2 cm, semicircle radius 0.5 cm).

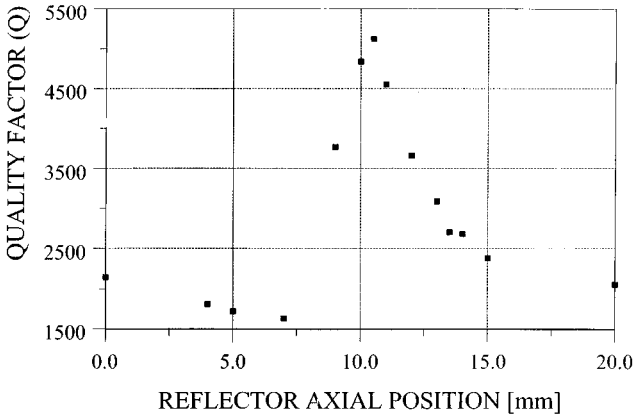
that in the frequency range of interest there are two modes with relatively narrow resonances, that in the width of the resonance is less than the separation between resonances. The two neighboring resonances correspond to two different axial modes of the structure. Each mode can be associated with a wave number shift  $\Delta k_z$  from the  $\pi$  point. As the frequency of the mode depends on the location of the reflector plate, so must the wave number shift.

Fig. 6(a) displays the dependence of mode frequency for the highest frequency mode on reflector position, while Fig. 6(b) shows the dependence of the quality factor. We note that as the reflector position is moved from 7 to 10 mm there is a sudden jump in mode frequency and simultaneously a sharp increase in the  $Q$ -factor. The increase in quality factor can be associated with the increase in frequency. As the mode frequency is raised, the operating point on the dispersion diagram approaches the  $\pi$  point. Consequently, the group velocity is lowered and the reflection coefficient increases.

This interpretation is confirmed on examination of the axial dependence of the field  $|H_\theta|$  profiles displayed in Fig. 7. Fig. 7(a) shows the case in which the reflector is at 0 mm while Fig. 7(b) shows the case in which it is at 10 mm. The field profile has the shape of a half sinusoid in Fig. 7(a) corresponding to  $\Delta k_z = \pi/L$ , while in Fig. 7(b) it is more in the character of a quarter sinusoid that would correspond to  $\Delta k_z = \pi/(2L)$ . We note that, in both cases, the field magnitude becomes relatively small at the output end of the structure. This is a manifestation of the fact that the transverse field profile in the structure is a poor match to that in a smooth waveguide. Consequently, there is a large reflection coefficient even though the output end is open. A similar phenomenon can be expected to occur at the input end. The shift of the shortening plate with respect to the beginning of the periodic structure leads to a phase shift between forward and backward waves as well as to a phase shift between harmonics of each wave. Changing of boundary conditions at the cathode end of the structure may lead to changing of the efficiency of device operation in addition to changing of the operating frequency, similar to the single-mode BWO case studied in [16] and [17]. In fact, it is clear from the nonsinusoidal dependence of mode frequency on



(a)



(b)

Fig. 6. Calculated (a) resonant frequency and (b)  $Q$ -factor of surface-wave mode of the resonator as a function of reflector position.

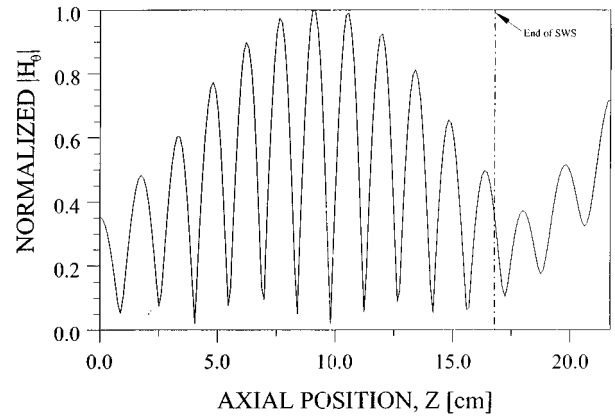
reflector position that reflections occur both at the end of the slow wave structure and at the reflector. Experimental results confirming this behavior and its effects on operating frequency and efficiency will be discussed in Section III.

#### E. Starting Current of a Surface-Wave Generator

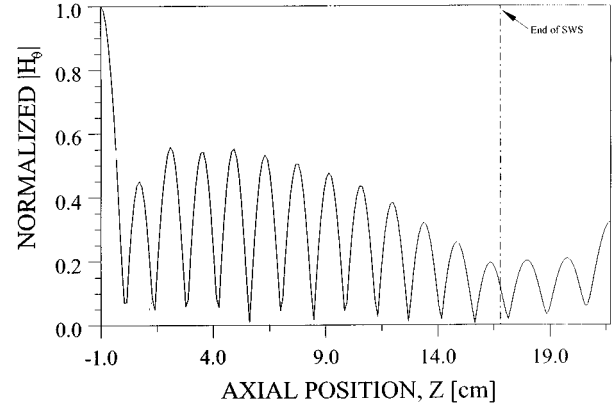
The effective mode selection in our surface wave generator is a result of operation near the upper cutoff of the  $TM_{01}$  mode. In this case, both forward and backward waves interact synchronously with the beam [18]. Actually, the influence of forward wave might be significant even for BWO operating far from  $\pi$  point [19]. Due to large reflection coefficient the calculated quality factor is significantly larger than minimal diffractive quality factor ( $Q_{\min D} \approx 2\omega L/v_g$ ). Under these circumstances the interaction between the fields and the electron beam can be calculated in the fixed field profile approximation. Based on the theory of a BWO operating near cutoff [18], the starting current of device operating with a half sinusoidal field profile ( $\Delta k_z = \pi/L$ ) [appropriate to the field distribution presented in Fig. 7(a)] is

$$I_{\text{start}} = \frac{I_A}{\pi N^2} \frac{\beta_z^3 \gamma^3}{C(r_b)} \frac{1}{Q} \frac{1}{\eta_{\text{Lin}}} \quad (6)$$

where  $N$  is the number of periods of structure,  $\beta_z$  is the longitudinal electron velocity normalized to the speed of light,  $C(r_b)$



(a)



(b)

Fig. 7. Calculated longitudinal distribution of  $|H_\theta|$  of  $TM_{01}$  mode of open resonator for two reflector positions: (a)  $\Delta z = 0$  cm (half of sinusoid envelop) and (b)  $\Delta z = 10$  cm (quarter of sinusoid envelop).

is the coupling coefficient introduced in [20],  $\eta_{\text{Lin}}$  is the linear efficiency given by

$$\eta_{\text{Lin}} = \left( \frac{\delta_+}{\delta_-} - 1 \right) \Phi \left( \delta_+ \frac{L}{2} \right) + \left( \frac{\delta_-}{\delta_+} - 1 \right) \Phi \left( \delta_- \frac{L}{2} \right) \quad (7)$$

where

$$\delta_+ = \frac{\pi}{L} - \frac{\pi}{d} - \frac{\omega}{c\beta_z}, \quad \delta_- = \frac{\pi}{L} + \frac{\pi}{d} - \frac{\omega}{c\beta_z}$$

$$\Phi(x) = \frac{d}{dx} \left( \frac{\sin^2 x}{x^2} \right).$$

The starting current as a function of beam voltage is plotted in Fig. 8 for the parameters corresponding to the parameters of the optimal design. For beam voltage in the range from 500 to 600 kV the calculated value of the starting current is about 1 kA. This value of the starting current is very attractive, since it corresponds to an optimal operating current of several kiloamperes.

When the beam current becomes large such that the reduced plasma frequency of the electron beam is comparable to the inverse transit time of electrons, space charge effects reduce the linear efficiency of interaction. To estimate this effect, we used an analytical technique similar to the one presented in [21].

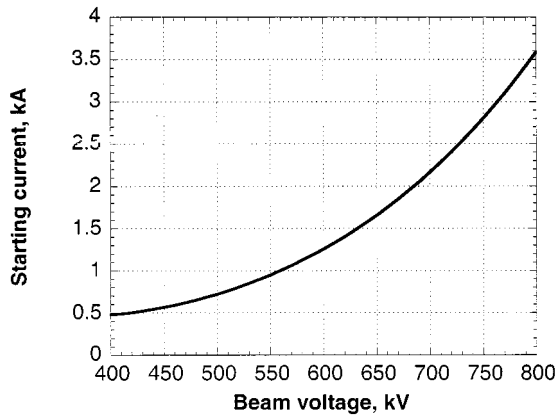


Fig. 8. Starting current of the surface-wave generator as a function of beam voltage (kV) for beam radius  $r_b = 4$  cm (12 periods, zero position of reflector).

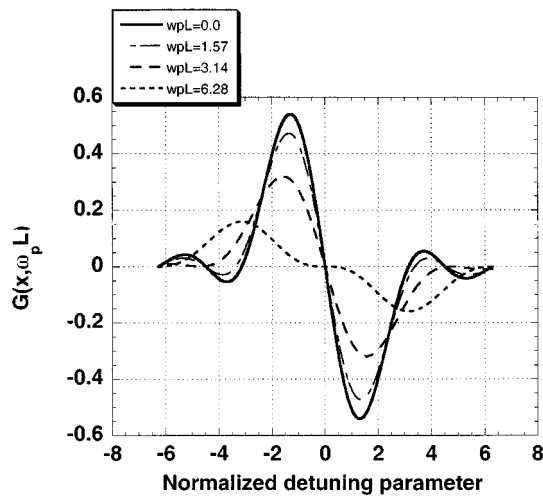


Fig. 9. Space charge effects: calculated values of  $G$  as a function of normalized detuning parameter for different values of the normalized reduced plasma frequency  $\omega_p L/2$ .

When the space charge effects are taken into account the function  $\Phi(\delta_{\pm}L/2)$  in the starting current expression (7) is replaced by function  $G(\delta_{\pm}L/2, \omega_p L/2)$

$$G(x, y) = \frac{1}{4y} \left[ \frac{\sin^2(x-y)}{(x-y)^2} - \frac{\sin^2(x+y)}{(x+y)^2} \right] \quad (8)$$

where  $\omega_p$  is the reduced plasma frequency of the electron beam. To illustrate the space charge effect the set of curves for different  $\omega_p L$  is presented in Fig. 9. As seen from the figure, the function  $G$  transforms to  $\Phi$  for small values of the beam-reduced plasma frequency. For large values of the reduced plasma frequency, space charge effects tend to reduce the linear efficiency of interaction in addition to the well-known shift of optimal the detuning.

For geometry and parameters selected here, the influence of space charge effects on the starting current is relatively small because the coupling coefficient is high and the interaction region is short ( $\omega_p L < 1.57$ ). Note that, in general, when  $Q$ -factors and/or coupling coefficients are small, space charge effects may preclude excitation of surface-waves.

As follows from expressions (6)–(8), the starting current is inversely proportional to linear efficiency. The linear efficiency

of the nonsymmetric  $\text{EH}_{mn}$  mode will be half the linear efficiency of the axially symmetric mode  $\text{TM}_{0n}$ , [22]. Here, we assume that the initial perpendicular velocity of electrons is negligible in comparison to their longitudinal velocity. In addition, the coupling coefficient for the  $\text{EH}_{mn}$  mode should be smaller than that of the  $\text{TM}_{0n}$  mode because for the same value of synchronous field  $E_z$  the nonsymmetric mode contains additional components contributing to stored energy. So, if the operating current of surface-wave generator is near optimal value  $I_{\text{opt}} = (3 \div 5)I_{\text{start}}$ , the  $\text{TM}_{01}$  mode will dominate over  $\text{EH}_{11}$  mode.

### III. EXPERIMENTAL SETUP AND RESULTS

The experimental setup is shown in Fig. 4 and briefly described in Section II. Pulses of 460–580 kV with time duration of 150 ns, drive a coaxial, magnetically insulated field emission gun. A longitudinal magnetic field was created by 1-m long pulse solenoid. In the experiments, strength of longitudinal magnetic field was about 2 torr. Various anode–cathode gaps were used, where in all of them, the cathode radius is 4 cm. In most cases, the cathode–anode gap is 10 cm, three times larger than the radial separation between the cathode and the external cylindrical section leading to the anode (3.3 cm) (the anode also acts as a reflector). The maximum current of an annular beam generated in a coaxial magnetically insulated gun under these conditions was obtained in [23] and is often referred to as Fedosov current. For the case of  $\gamma \cong 2$ , Fedosov current is about three-quarters of the vacuum limiting current of a beam with the same parameters. For the driving voltages specified above, an annular electron beam of 5.8 kA was produced. As already known, by decreasing the cathode–anode gap, it is possible to increase significantly the beam current. In our experiment, it was possible to increase the injected beam current up to 16.8 kA when the anode–cathode gap was 3 cm. The background vacuum was  $10^{-5} \div 10^{-6}$  torr.

The radial position of the beam can be changed in the range from 35 to 39 mm by using magnetic compression. The thickness of the beam was measured by a thermally sensitive damage pattern, and found to be approximately 1 mm. This diagnostic enabled alignment of the beam with respect to the slow-wave structure with accuracy of  $\sim 0.5$  mm.

The microwave radiation was extracted through an output section, which is composed of two regions (see Fig. 4). The first region consists of an up-taper and a coaxial beam collector [24]. The collector design is important for the operation of high-current surface-wave generator because the beam current is a substantial fraction of the vacuum limiting current inside the SWS. The limiting current in the output section is smaller than the desired operating current. Therefore, we designed a collector capable of preventing reflection of electrons back into the interaction region. This stainless steel-graphite collector held by three thin metallic fins has an inner radius of 3.5 cm, thickness of 1 cm, and is located 5 cm down from the edge of the slow-wave structure in the region of uniform magnetic field. The actual collector geometry was designed to maximize beam collection efficiency and minimize interference with microwave propagation. The collector was immersed in a strong guiding

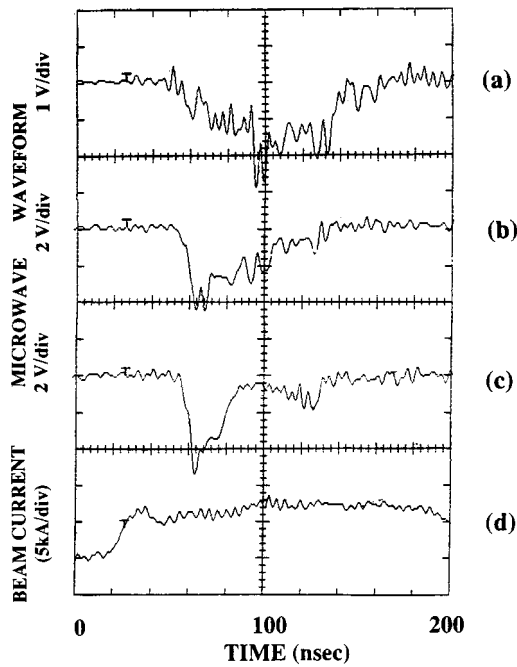


Fig. 10. Microwave signal measured by hot carrier detector and beam current as a function of time for  $V_b = 500$  kV: (a) total radiated energy 5J, (b) total radiated energy 6.7J, (c) total radiated energy 10.2J, and (d) beam current. Microwave energy was measured calorimetrically. Microwave waveform was measured by the hot carrier detector mounted behind the calorimeter (see Fig. 4).

magnetic field. After hundreds of shots, the output window did not suffer any damages due to either surface breakdown or electrons. The second region of the extraction section is a large-diameter (64 cm) output window.

The diagnostics of the microwave radiation included four separate measurements:

- 1) large cross-section calorimeter to measure the total radiated energy [25] (mounted close to the output window, on the airside, see Fig. 4);
- 2) hot carrier and diode detectors for waveform detection [26] (mounted behind the calorimeter, see Fig. 4);
- 3) polarization measurement (through rotation of the pickup horns, see Fig. 4);
- 4) dispersive line to measure the frequency.

Typical waveforms of microwave output signals and of the injected beam current are shown in Fig. 10(a)–(d). The top three traces in Fig. 10(a)–(c), are microwave signals, measured by hot carrier detectors, for three different axial positions of the reflector, namely, 20, 23, and 21.5 mm. The fourth trace in Fig. 10(d) is the injected beam current, as measured by a Rogowski current monitor. Both the microwave power and the pulse shape depend on the axial position of the reflector. A more detailed description of the peak detector power as a function of the axial position of the reflector position is presented in Fig. 11. Two distinct peaks at 4 and 21.5 mm are clearly seen, pointing to two different modes of operation. The simulations predicted a similar behavior (see Fig. 7), where the two axial positions of the reflector correspond to two different axial modes. The axial position of the reflector also affects the radiation frequency, as can be seen in Fig. 12. The

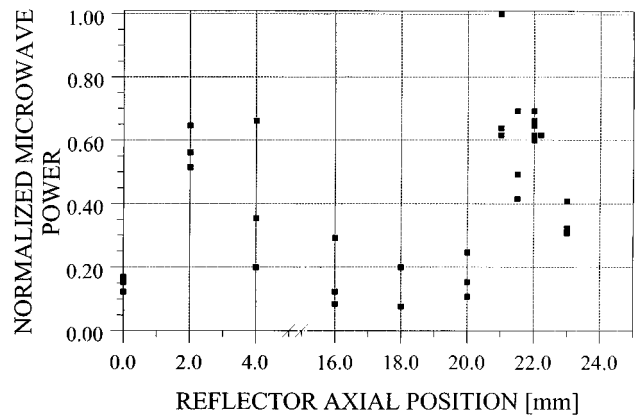


Fig. 11. Measured dependence of the normalized microwave power on axial position of the reflector (500 kV, 5.8 kA).

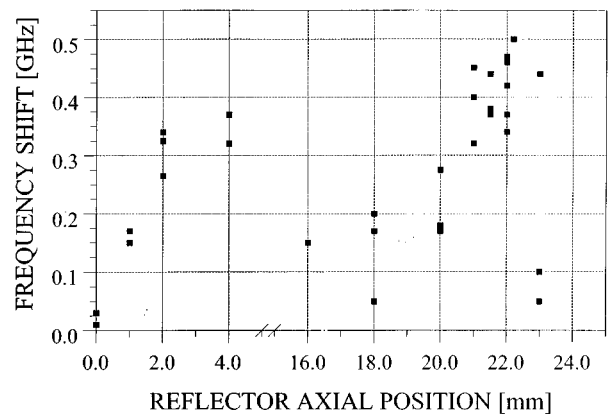


Fig. 12. Measured frequency shift as a function of the axial position of the reflector (500 kV, 5.8 kA).

frequency in the high-efficiency regime (reflector positioned at 21 mm), is higher by about 300 MHz than the frequency in the low-efficiency regime (reflector positioned at 16 mm). The axial adjustment of the reflector enables about 3.6% frequency tunability, and 1:4 power tunability for fixed voltage and current of the beam.

The total radiated energy was calorimetrically measured as a function of the axial position of the reflector. The results are summarized in Table I. In these experiments, the highest radiated power 0.5 GW was obtained for a beam voltage of 570 kV and current of 5.8 kA, namely, efficiency of 15%. The radiated waveform is shown in Fig. 10 for three levels of output power, namely, a) 0.15 GW, b) 0.21 GW, and c) 0.47 GW. It is evident from these traces that an increase in the radiated power is accompanied by reduction of the pulse duration, hence, the maximum output power is restricted by the pulse-shortening effect. We also observed that after several hundred shots, the middle section of the SWS was covered by hundreds of spots. The distribution of the spots was azimuthally homogeneous. Most of the spots were localized on the semicylindrical surfaces of the slow wave structure, where the calculated (using PIC code) strength of the axial component of the RF electric field  $E_z$  is the largest, and in excess of 400 kV/cm. There are few mechanisms that can lead to pulse shortening. In this work, surface breakdown seems to be a candidate because the calculated surface field are

TABLE I  
TOTAL MICROWAVE RADIATED POWER AS A FUNCTION OF AXIAL POSITION OF INTERNAL REFLECTOR

Axial position of reflector (mm)	0	2	4	21.5	23
Total radiated energy (J)	4.4-5.8	6.2-7.2	3.3-3.8	9-10.2	6.2-7.2
Peak power (GW)	0.14	0.2-0.35	0.14-0.16	0.47-0.5	0.22-0.29

well above the field emission threshold. Furthermore, the surface field intensity is maximized in the middle of the structure.

Increasing the injected beam current to 16.8 kA (at 460 kV) did have very little effect on the total radiated microwave energy and waveform, but substantially downshifted the operating frequency by about 500 MHz.

#### IV. SUMMARY AND CONCLUSION

In this work, we presented theoretical and preliminary experimental results of a large cross section, GW class HPM source. The device is intended to be driven by an electron beam of a modest voltage ( $\sim 500$  kV), which is an important feature for practical uses. We found that an overmoded interaction cavity must support surface wave that are synchronous with the electron beam, and simultaneously exhibit large values of the coupling impedance. The surface waves are crucial in order to avoid mode competition, while large coupling impedance is important to obtain high efficiency interaction. We found that a periodic structure that is combined of semicircles on top of rectangles satisfies both requirements.

An adjustable internal reflector separates the electron gun from the interaction region. Both our simulations and experimental results show that a small axial adjustment of the reflector positions dramatically change the electrodynamic properties of the cavity. We found that both the quality factor and resonance frequency are strongly dependent on the axial position of the reflector. Furthermore, depending on the axial position, different modes are excited in the cavity, thus different field profiles are obtained. The starting current, for the preferred SWS and beam voltage of 500 kV, is estimated to be about 1 kA.

The experimental setup was based on the theoretical studies, and included a coaxial magnetically insulated electron field emission gun, a 12-period SWS, and a coaxial coupler for efficient energy extraction. The electron gun was driven by pulses of 460–580 kV, 150 ns duration, and produced from 5.8 to 16.8 kA annular beam. The coaxial coupler was placed in order to improve the extraction of microwave power, and the beam collection. Preliminary PIC simulations have shown that without the coaxial coupler the electrons got trapped at the up-taper section and the beam was partly reflected to the interaction region. The emitted power level and the efficiency were dramatically reduced.

Both the frequency and radiated power level of the microwaves were found to be strongly dependent on the axial position of the internal reflector. We detected two distinct peaks of the radiating power when the reflector was shifted up to about 25 mm away from the edge of the SWS. We concluded that tuning of the radiated power, efficiency, and frequency

is possible, for fixed beam parameters, by adjusting the axial position of the reflector.

At the optimal position of the reflector, peak power levels of 0.5 GW, total radiated microwave energy of 10.2 J, and efficiency of 15% were measured at 8.3 GHz. A pulse-shortening effect accompanied the increment in the radiated power. After several hundred shots, we discovered hundreds of spots uniformly distributed on the internal surface of the SWS. Increasing the beam current to 16.8 kA had small effect on the radiated power, but downshifted the frequency by 500 MHz.

In conclusion, we have demonstrated single-mode operation of a large-diameter surface wave generator. Our results prove that moderate voltage electron beams can drive gigawatt level radiation sources, and that peak power is still restricted by the pulse-shortening effect. Additional optimization of the extraction section (coaxial and output window regions) is required in order to increase the radiated power and energy. Alternatively, further increase of the transverse cross section may enable the generation of higher levels of microwave power.

#### APPENDIX A LIMITING BEAM POWER

To estimate the maximum beam power of a thin annular electron beam of radius  $r_b$  propagating in a smooth waveguide of a radius  $r_w$ , we start from the energy conservation law for an electron moving inside a smooth waveguide. As follows from the energy conservation law, the sum of potential and kinetic energies of the electron should be equal to a kinetic energy of the injected electron

$$(\gamma_b - 1)mc^2 + q\Phi = (\gamma_a - 1)mc^2 \quad (\text{A1})$$

where  $\gamma_a = 1 + eV_{ac}/mc^2$  corresponds to the anode-cathode voltage  $V_{ac}$ ,  $\gamma_b$  is the actual electron's energy normalized to the rest energy which is smaller than  $\gamma_a$  due to the voltage depression effect,  $\Phi$  is an electrostatic potential, and  $q$  is the electron charge. The well-known electrostatic solution for a thin annular beam inside a conducting cylinder is [8]

$$\Phi(r_b) = -2 \frac{I_b}{v_{b,z}} \ln\left(\frac{r_w}{r_b}\right) \quad (\text{A2})$$

where  $v_{b,z}$  is a longitudinal beam velocity. This leads us to an expression for a beam current

$$\begin{aligned} I_b &= \frac{mc^2}{e} \frac{1}{2 \ln(r_w/r_b)} v_{b,z} (\gamma_a - \gamma_b) \\ &= I_A \frac{1}{2 \ln(r_w/r_b)} (\gamma_b^2 - 1)^{1/2} \left( \frac{\gamma_a}{\gamma_b} - 1 \right) \end{aligned} \quad (\text{A3})$$

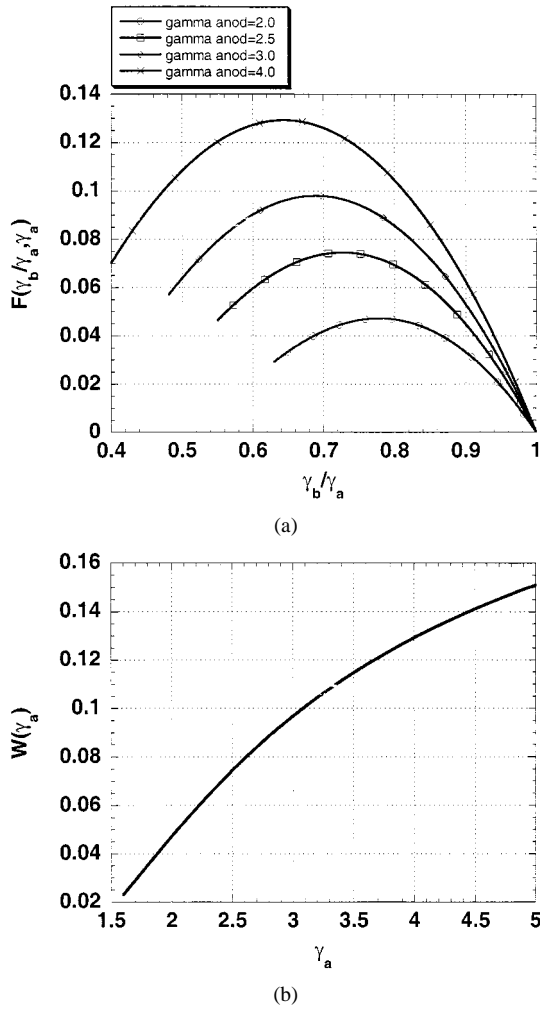


Fig. 13. Voltage depression effects: (a)  $F$  as a function of  $\gamma_b/\gamma_a$ , for different values of  $\gamma_a$  (labeled as *gamma anod*), and (b)  $W$  as a function of  $\gamma_a$ .

where  $I_A = 17.04$  kA. The electron beam power corresponding to this value of the beam current  $I_b$  and voltage  $V_b$  is

$$\begin{aligned} P_b &= I_b V_b = I_b \frac{mc^2}{e} (\gamma_b - 1) \\ &= I_A \frac{1}{2\ln(r_w/r_b)} \gamma_a^2 F\left(\frac{\gamma_b}{\gamma_a}, \gamma_a\right) U_0 \end{aligned} \quad (\text{A4})$$

where  $U_0 = 511$  kV, and

$$F\left(\frac{\gamma_b}{\gamma_a}, \gamma_a\right) = \left(\frac{\gamma_b}{\gamma_a} - \frac{1}{\gamma_a}\right)^{3/2} \left(\frac{\gamma_b}{\gamma_a} + \frac{1}{\gamma_a}\right)^{1/2} \left(\frac{\gamma_a}{\gamma_b} - 1\right). \quad (\text{A5})$$

The dependence of  $F(\gamma_b/\gamma_a, \gamma_a)$  on the ratio  $\gamma_b/\gamma_a$  for different values of  $\gamma_a$  is presented at Fig. 13(a). As it seen from figure the function  $F(\gamma_b/\gamma_a, \gamma_a)$  approaches maximum value at different values of  $\gamma_b/\gamma_a$  for different  $\gamma_a$ .

To find the limiting value of the electron beam power for given geometry and given value of  $\gamma_a$  it is necessary to find maximum values of  $F(\gamma_b/\gamma_a, \gamma_a)$  for each  $\gamma_a$ . We introduce function  $W(\gamma_a)$

$$W(\gamma_a) = \max[F(\gamma_b/\gamma_a, \gamma_a)]. \quad (\text{A6})$$

The dependence of the function  $W(\gamma_a)$  on  $\gamma_a$  is plotted in Fig. 13(b). After this, the expression (2) for the maximum beam power follows from (A4)–(A6):

$$\begin{aligned} P_{b,\text{lim}} &= I_A U_0 \frac{1}{2\ln(r_w/r_b)} \gamma_a^2 \max\left[F\left(\frac{\gamma_b}{\gamma_a}, \gamma_a\right)\right] \\ &= \frac{8.707 \cdot 10^9 \text{ [W]}}{2\ln(r_w/r_b)} \gamma_a^2 W(\gamma_a). \end{aligned} \quad (\text{A7})$$

#### ACKNOWLEDGMENT

The authors are grateful for J. Pyle and D. Cohen for their invaluable help with the experimental apparatus.

#### REFERENCES

- [1] F. J. Agee, "Evolution of pulse shortening research in narrow band high power microwave sources," *IEEE Trans. Plasma Sci.*, vol. 26, pp. 235–245, June 1998.
- [2] S. P. Bugaev, V. I. Kanavets, A. I. Klimov, V. I. Koshelev, and V. A. Cherepenin, "Relativistic multiwave Cerenkov generator," *Sov. Tech. Phys. Lett.*, vol. 9, no. 11, pp. 596–597, 1983. (originally published in *Pis'ma Zh. Tekh. Fiz.*, vol. 3, no. 13, pp. 1385–1389, 1983).
- [3] S. P. Bugaev, V. I. Kanavets, A. I. Klimov, V. I. Koshelev, A. I. Slepov, and V. A. Cherepenin, "Interaction of an electron beam and an electromagnetic field in multiwave  $10^{10}$ W Cerenkov generator," *Sov. J. Commun. Tech. Electr.*, vol. 32, no. 11, pp. 79–87, 1987.
- [4] D. K. Abe, Y. Carmel, S. M. Miller, A. Bromborsky, B. Levush, T. M. Antonsen, Jr., and W. Destler, "Experimental studies of overmoded relativistic backward-wave oscillators," *IEEE Trans. Plasma Sci.*, vol. 26, pp. 591–604, June 1998.
- [5] S. P. Bugaev, V. A. Cherepenin, V. I. Kanavets, V. I. Koshelev, V. A. Popov, and A. N. Vlasov, "Investigation of a millimeter-wavelength-range relativistic diffraction generator," *IEEE Trans. Plasma Sci.*, vol. 18, pp. 518–524, June 1990.
- [6] S. P. Bugaev, V. A. Cherepenin, V. I. Kanavets, A. I. Klimov, A. D. Kopenkin, V. I. Koshelev, V. A. Popov, and A. I. Slepov, "Relativistic multiwave Cerenkov generators," *IEEE Trans. Plasma Sci.*, vol. 18, pp. 525–536, June 1990.
- [7] A. V. Gunin, A. I. Klimov, S. D. Korovin, I. K. Kurkan, I. V. Pegel, S. D. Polevin, A. M. Roitman, V. V. Rostov, A. S. Stepchenko, and E. M. Totmeninov, "Relativistic X-band BWO with 3-GW output power," *IEEE Trans. Plasma Sci.*, vol. 26, pp. 326–331, June 1998.
- [8] R. B. Miller, *An Introduction to the Physics of Intense Charged Beams*. New York: Plenum, 1982.
- [9] V. L. Bratman, G. G. Denisov, M. M. Ofitserov, S. D. Korovin, S. D. Polevin, and V. V. Rostov, "Millimeter-wave HF relativistic electron oscillators," *IEEE Trans. Plasma Sci.*, vol. 15, pp. 2–15, Feb. 1987.
- [10] V. L. Bratman, G. G. Denisov, N. S. Gingburg, A. V. Smorgonsky, S. D. Korovin, S. D. Polevin, V. V. Rostov, and M. I. Yalandin, "Stimulated scattering of waves in microwave generators with high-current relativistic electron beams: Simulation of two stage free-electron laser," *Int. J. Electron.*, vol. 59, no. 3, pp. 247–289, 1985.
- [11] V. L. Bratman, G. G. Denisov, B. D. Kolchugin, S. D. Korovin, S. D. Polevin, and V. V. Rostov, "Powerfull millimeter-wave generators based on the stimulated Cerenkov radiation of relativistic electron beam," *Int. J. Infrared Millimeter Waves*, vol. 5, pp. 1411–1332, 1984.
- [12] A. F. Alexandrov, S. Yu. Galuzo, V. I. Kanavets, and V. A. Pletyushkin, "Surface wave excitation by electron flow in a diaphragmatic waveguide," *Sov. J. Tech. Phys.*, vol. 51, no. 8, pp. 1727–1730, 1981.
- [13] S. Humphries, Jr., *Field Solution on Computers*. Boca Raton, FL: CRC, 1997.
- [14] Y. Carmel, H. Guo, W. R. Lou, D. Abe, V. L. Granatstein, and W. W. Destler, "Novel method for determining the electromagnetic dispersion relation of periodic slow wave structure," *Appl. Phys. Lett.*, vol. 57, no. 13, pp. 1304–1306, 1990.
- [15] I. Y. Gushchina and V. M. Pikunov, "Numerical method of analyzing electromagnetic fields of periodic waveguides," *Sov. J. of Commun. Tech. Electr.*, vol. 37, no. 16, pp. 50–59, 1992.

- [16] L. D. Moreland, E. Shamiloglu, R. W. Lemke, A. M. Roitman, S. D. Korovin, and V. V. Rostov, "Enhanced frequency agility of high-power relativistic backward wave oscillators," *IEEE Trans. Plasma Sci.*, vol. 24, pp. 852–858, June 1996.
- [17] A. N. Vlasov, G. S. Nusinovich, and B. Levush, "Effect of the zero spatial harmonic in a slow electromagnetic wave on operation of relativistic backward-wave oscillators," *Phys. Plasmas*, vol. 4, no. 5, pp. 1402–1412, 1997.
- [18] S. M. Miller, T. M. Antonsen Jr., B. Levush, A. Bromborsky, D. K. Abe, and Y. Carmel, "Theory of relativistic backward wave oscillators operating near cutoff," *Phys. Plasmas*, vol. 1, pp. 730–740, 1994.
- [19] S. D. Korovin, S. D. Polevin, A. M. Roitman, and V. V. Rostov, "Influence of the traveling wave on efficiency of the relativistic BWO," *Sov. Tech. Phys. Lett.*, vol. 20, pp. 12–16, 1994.
- [20] B. Levush, T. M. Antonsen Jr., A. Bromborsky, W. R. Lou, and Y. Carmel, "Relativistic backward-wave oscillators: Theory and experiment," *Phys. Fluids*, vol. B4, pp. 2293–2299, 1992.
- [21] M. I. Petelin, "Space-charge effects in the excitation of a cavity resonator by steady flow of excited classical oscillators," *Radiophys. Quantum. Electron.*, vol. 28, pp. 239–245, 1985.
- [22] A. N. Vlasov, A. S. Il'in, and V. A. Cherepenin, "Multiwave interaction of relativistic electron flux with electrodynamic structure fields in weak-signal mode," *Bull. Russian Acad. Sci.*, vol. 62, no. 12, pp. 1964–1971, 1998.
- [23] A. I. Fedosov, E. A. Litvinov, S. Ya. Belomytsev, and S. P. Bugaev, "Characteristics of electron beam formed in diodes with magnetic insulation," *Sov. Phys. J.*, vol. 20, no. 10, pp. 1367–1368, 1977.
- [24] S. A. Naqvi, G. S. Kerslick, J. A. Nation, and L. Schachter, "Axial extraction of high-power microwaves from relativistic traveling wave amplifiers," *Appl. Phys. Lett.*, vol. 69, no. 11, pp. 1550–1552, 1996.
- [25] A. Shkvarunets, S. Kobayashi, Y. Carmel, J. Rodgers, T. Antonsen Jr., and V. Granatstein, "A broad band (4–25 GHz) calorimeter for diagnostic high power microwave sources," in *Proc. IEEE Conf. Rec., IEEE Int. Conf. Plasma Sci.*, Monterey, CA, June 1999, p. 170. (Paper 3P19).
- [26] M. Dazyg, Z. Kanchleris, V. Orsherskis, and R. Summiskis, "Resistive sensor for high short pulse microwave measured in waveguides," *Electron. Lett.*, vol. 31, no. 3, pp. 1355–1357, 1995.



**Alexander N. Vlasov** (M'95) was born in Lipetskaya Oblast, Russia, in 1958. He received the B.Sc. (honored), M.S., and Ph.D. degrees in physics from Moscow State University, Moscow, Russia, in 1981, 1986, and 1987, respectively.

After graduation, he was a Research Scientist from 1986 to 1991, an Assistant Professor from 1991 to 1995, and an Associate Professor since 1995 at Department of Physics of Moscow State University. From 1991 to 1998, he was a Visiting Scientist at the Institute for Plasma Research of

University of Maryland, College Park. In 1999, he joined Science Applications International Corporation, McLean, VA. His current research interests include the theory, computer simulations, and design of high-power sources of coherent microwave- and millimeter-wave radiation, computational methods in diffraction theory, and the theory of electromagnetic fields in complex media.

**Anatoly G. Shkvarunets** received the B.Sc. degree in physics from Moscow State University, Moscow, Russia, in 1970. He held a Lebedev Physical Institute Graduate Fellowship from 1972 to 1975 and received the Ph.D. degree in physics in 1977 from the same institute.

Since 1975, he has been a Junior and then Senior Research Associate at Lebedev, and later, at the General Physics Institute, Moscow. He has been an investigator of relativistic electron beam (REB) plasma interaction for REB transport plasma heating and microwave oscillation as well as plasma characterization and plasma-wave excitation. Since 1994, he has been a Visiting Scientist in the Institute for Plasma Research at the University of Maryland, College Park. He has given over 20 conference presentations and published over 40 papers in the area of REB-plasma interaction and high-power microwaves.



**John C. Rodgers** received the B.S. degree in electrical engineering from the University of Maryland, College Park, in 1985 and is currently working towards the Ph.D. degree with his dissertation titled, "Phase Control and Coherence in Harmonic, Frequency-doubling Gyro-amplifiers."

He served in the United States Navy from 1975 to 1981, where he worked on satellite and UHF communications and radar navigation systems. In 1985, he joined the Institute for Plasma Research at the University of Maryland and has served as the Associate

Director since 1996. He has worked on the propagation and applications of intense relativistic particle beams, collective ion acceleration, large orbit gyrotrons, broad-band plasma-microwave interactions, free electron lasers, pulse power design and applications, and relativistic plasma electronic devices. More recently, his activities include experimental studies of harmonic gyro-oscillators and amplifiers with an emphasis on phase control of the output radiation, a gigawatt surface-wave oscillator and high-efficiency vacuum electronic amplifiers. He has authored or coauthored more than 60 journal articles and is a contributing author of the book, *Advances in High Power Microwave Sources and Techniques* (Piscataway, NJ: IEEE Press), to be published.

**Yuval Carmel** (S'66–M'69–SM'90) was born in Israel in 1942. He received the B.Sc. and M.S. degrees from the Technion–Israel Institute of Technology, Haifa, Israel, in 1966 and 1971, respectively, and the Ph.D. degree from Cornell University, Ithaca, NY, in 1974, all in electrical engineering.

He was with the Israeli government for 15 years, the Naval Research Laboratory, Washington DC, from 1981 to 1983, and has been with the University of Maryland, College Park, since 1988. His research interests include electromagnetic radiation from intense electron beams, plasma microwave devices, advanced concepts in millimeter-waves tubes, gyrotrons, and backward-wave oscillators.



**Thomas M. Antonsen, Jr.** (M'87) was born in Hackensack, NJ in 1950. He received the Bachelor's degree in electrical engineering in 1973, and his Master's and Ph.D. degrees in 1976 and 1977, all from Cornell University. He was a National Research Council Post Doctoral Fellow at the Naval Research Laboratory in 1976–1977, and a Research Scientist in the Research Laboratory of Electronics at MIT from 1977 to 1980. In 1980, he moved to the University of Maryland where he joined the faculty of the departments of Electrical Engineering and Physics in 1984. He is currently a Professor of Physics and Electrical Engineering. He has held visiting appointments at the Institute for Theoretical Physics (U.C.S.B.), the Ecole Polytechnique Federale de Lausanne, Switzerland, and the Institute de Physique Theorique, Ecole Polytechnique, Palaiseau, France. He was selected as a Fellow of the Division of Plasma Physics of the American Physical Society in 1986.

Prof. Antonsen's research interests include the theory of magnetically confined plasmas, the theory and design of high power sources of coherent radiation, nonlinear dynamics in fluids, and the theory of the interaction of intense laser pulses and plasmas. He is the author and coauthor of more than 180 journal articles and coauthor of the book *Principles of Free-electron Lasers*. He has served on the editorial board of *Physical Review Letters*, *The Physics of Fluids*, and *Comments on Plasma Physics*.

**Tamer M. Abuelfadl**, photograph and biography not available at the time of publication.

**Duan Lingzi**, photograph and biography not available at the time of publication.



**Vladimir A. Cherepenin** (M'99) was born in Moscow, Russia, on August 14, 1947. He graduated from the Physics Department of Moscow State University, where he also received the Ph.D. degree in physics and mathematics in 1979. In 1989, he received the Prof. Dr. degree in physics from the Institute of Radio Engineering and Electronics of the Russian Academy of Sciences.

Since 1985, he has been the Head of Computational Physics Laboratory of the Institute of Radio Engineering and Electronics and is a Professor since

1997. His research interests include high-power microwave devices and their applications, free electron lasers, transformation of explosion energy into coherent electromagnetic radiation, and the application of computational physics methods to studying processes in interacting media. He is author of more than 100 journal articles and one book.



**Gregory S. Nusinovich** (SM'92-F'00) was born in Berdichev, Russia. He received the B.Sc., M.S., and Ph.D. degrees from Gorky State University, Russia, in 1967, 1968, and 1975, respectively.

In 1968, he joined the Gorky Radiophysical Research Institute. From 1977 to 1990, he was a Senior Research Scientist and Head of Research Group at the Institute of Applied Physics of the Academy of Sciences of the U.S.S.R. From 1968-1990, his scientific interests were aimed at developing high-power millimeter- and submillimeter-wave gyrotrons. In 1991,

he emigrated to the United States, where he joined the research staff at the Institute for Plasma Research, University of Maryland, College Park. Since 1991, he has also served as a Consultant to the Science Applications International Corporation, the Physical Science Corporation, and Omega-P, Inc. In 1996, he was a Guest Co-Editor of the Sixth Special Issue of IEEE TRANSACTION ON PLASMA SCIENCE on High Power Microwave Generation and in 1999 he was Guest Co-Editor of the Special Issue of IEEE TRANSACTIONS ON PLASMA SCIENCE on Cyclotron Resonance Maser and Gyrotrons.

Dr. Nusinovich was a member of the Scientific Council on the Physical Electronics of the Academy of Sciences of the U.S.S.R. He currently served on the Editorial Board of the IEEE TRANSACTIONS ON PLASMA SCIENCE.

**Moti Botton**, photograph and biography not available at the time of publication.



**Victor L. Granatstein** (S'59-M'84-SM'86-F'92) received the Ph.D. degree in electrical engineering from Columbia University, NY, in 1963.

After a year of postdoctoral work at Columbia, he was a Research Scientist at Bell Telephone Laboratories from 1964 to 1972. In 1969-1970, he was a Visiting Senior Lecturer at the Hebrew University of Jerusalem. In 1972, he joined the Naval Research Laboratory (NRL), Washington, DC, as a Research Physicist, and from 1978 to 1983, he served as Head of NRL's High Power Electromagnetic Radiation

Branch. In August 1983, he became a Professor in the Electrical Engineering Department of the University of Maryland, College Park. From 1988 to 1998, he was Director of the Institute for Plasma Research at the University of Maryland. In 1994, he spent a semester as a Visiting Professor at the University of Tel Aviv, Israel. He is presently leading studies of electromagnetic radiation from relativistic electron beam and advanced concept in millimeter-wave tubes, especially gyrotron amplifiers. He has coauthored more than 200 research papers in scientific journals and has coedited three books. He holds a number of patents on active and passive microwave devices.

Dr. Granatstein is a Fellow of the American Physical Society. He has received a number of major research awards including the E.O. Hulbert Annual Science Award (1979), the Superior Civilian Service Award (1980), the Captain Robert Dexter Conrad Award for scientific achievement (awarded by the Secretary of the Navy, 1981), the IEEE Plasma Science and Applications Award (1991), and Robert L. Woods Award for Excellence in Electronics Technology (1998).